https://doi.org/10.5194/egusphere-2023-201
Preprint. Discussion started: 16 February 2023

An Overview of Solar Radio Type II Bursts through analysis of associated solar and near Earth space weather features during Ascending phase of SC 25

Theogene Ndacyayisenga[1,2], Jean Uwamahoro[3], Jean Claude Uwamahoro[1], Rabiu Babatunde[2], Daniel Okoh[2], Kantepalli Sasikumar Raja[4], Christian Kwisanga[1], and Christian Monstein[5]

[1]University of Rwanda - College of Science and Technology, Kigali, P.O.BOX 3900, Rwanda
[2]Center for Atmospheric Research, National Space Research and Development Agency, Anyigba, Nigeria
[3]University of Rwanda, College of Education, P.O. BOX 55, Rwamagana – Rwanda
[4]Indian Institute of Astrophysics, II Block, Koramangala, Bengaluru - 560 034, India
[5]IRSOL, Istituto Ricerche Solari "Aldo e Cele Daccò", Università della Svizzera italiana, Locarno, Switzerland.

Correspondence: Theogene Ndacyayisenga (ndacyatheogene@gmail.com)

Abstract. Type II solar radio bursts are the signatures of particle acceleration caused by shock waves in the solar atmosphere and interplanetary space. Being electromagnetic radiation that travel at the speed of light, they can serve as ground observed data to provide early notice of incoming solar storm disturbances. An observational overview of 31 Type II bursts which occurred in the period between May 2021 to December 2022 is made. We analyzed associated parameters such as bandwidth, drift rates, starting frequency to evaluate their dynamical parameters such as the shock and Alfvén speeds to estimate the Alfvén Mach number as well as the coronal magnetic field strength using Rankine-Hugoniot relation. We also evaluated accompanying space weather implication in terms of ionospheric total electron content (TEC) enhancement. At heliocentric distance $\sim 1-2\ R\odot$, the shock and the Alfvén speeds are in the range 504 - 1301 kms^{-1} and 368 - 837 kms^{-1}, respectively. The Alfvén Mach number is of the order of $1.2 \leq \mathrm{M_A} \leq 1.8$ at the same heliocentric distance, and the magnetic field strength shows excellent consistency and could be fit with a single power-law distribution of the type $B(r) = 6.56r^{-3.92}\ G$. The study finds that 15/31 type II radio bursts are associated with some aspects of space weather such as radio blackouts and/or polar cap absorption events, that are the signature of solar proton enhancement and solar energetic particle events. Observed and analyzed Type II events correlated well with observed ionospheric storm indicated by the TEC enhancement. The findings from this study indicate that through analysis of type II SRBs observed from the ground and their physical features characteristics, it is possible to monitor the current progress of solar cycle 25 and predict the intensity of associated space weather phenomena.

1 Introduction

The interaction of coronal mass ejections (CMEs) and their shocks with the magnetosphere is the major cause of strongest space weather effects. The energy release from explosive flares also causes perturbations in the Earth's atmosphere (Salmane et al., 2018; Vourlidas et al., 2020). The radio emissions that occur in the solar atmosphere to interplanetary space arise from a broad range of physical phenomena with space weather implications (e.g., flares, solar energetic particles, CMEs and shocks,

https://doi.org/10.5194/egusphere-2023-201
Preprint. Discussion started: 16 February 2023

Fleishman et al., 2020; Nindos, 2020; Vourlidas et al., 2020). Solar radio bursts (SRBs) originate from different altitudes in the solar atmosphere and they are observed over a wide range of wavelengths from millimeters to centimeters up to meters and decameters. Wild et al. (1963) classified SRBs into five types according to their morphologies of their dynamic spectra and their origin. Of the five types, type II, III and IV bursts are relevant to space weather study because they are associated with space weather drivers, such as shock waves (type II bursts, Cairns et al., 2003; Cane and Erickson, 2005; Chernov and Fomichev, 2021), streams of electrons propagating along open magnetic field lines (type III bursts, Reid and Ratcliffe, 2014, for a review) and CMEs or post-flare loops (type IV bursts, Nindos et al., 2008; Kumari et al., 2021). In the present paper, metric type II radio bursts observed from the ground by extended Compound Astronomical Low frequency Low cost Instrument for Spectroscopy and Transportable Observatory, herein, e-CALLISTO (Benz et al., 2005, 2009) are studied.

First discovered by Payne-Scott et al. (1947), type II radio bursts are among the most powerful events in the solar radio emission observed at metric wavelength (e.g., Wild and McCready, 1950). At present, it is generally accepted that type II radio emissions are excited by magnetohydrodynamic (MHD) shock waves driven by solar flares, CMEs and fast plasma flow in the magnetic reconnection regions (e.g., Maia et al., 2000; Pick et al., 2006; Temmer et al., 2010; Grechnev et al., 2011; Vasanth et al., 2011; Kumari et al., 2017; Gopalswamy et al., 2018; Zucca et al., 2018; Chernov and Fomichev, 2021). Physical properties of metric type II radio bursts including but not limited to drift rate, starting frequency and duration are used to study the dynamics of the middle and upper solar corona. For example, the Alfvén Mach number, $\mathrm{M_A} = \mathrm{V_S}/\mathrm{V_A}$, ($V_S$ and V_A, are shock and Alfvén speeds, respectively) is calculated in three different methods: (i) from shock geometry in EUV images, (ii) by the ratio of the CME speed to the Alfvén speed and (iii) using shock parameters derived from type II radio band-splitting phenomena (Vršnak et al., 2002). A recent study by Maguire et al. (2020) showed that these three methods give consistent results after their comparative analysis.

By analyzing one or two events, many authors (e.g., Cho et al., 2013; Cunha-Silva et al., 2015; Kumari et al., 2017; Maguire et al., 2020; Lata Soni et al., 2021; Kouloumvakos et al., 2021; Mann et al., 2022) have determined the magnetic field strengths and examined the spatial and temporal evolution of shock properties, as well as the conditions responsible for type II radio emissions during high solar activity of solar cycle 24. There have been few works completed during the rise and fall phases of solar cycle 24 (e.g., Gopalswamy and Yashiro, 2011; Vasanth et al., 2014). Kim et al. (2012), on the other hand, covered the entire solar cycle 23. In the current study, a number of events are analyzed during the ascending phase of solar cycle 25 which started in December 2019 (Kallunki et al., 2021; Ahluwalia, 2022; Brajša et al., 2022). We apply the Rankine-Hugoniot density jump relation and parameters of type II radio bursts to estimate the parameter of shock waves (shock and the Alfvén speed, the Alfvén Mach number) of metric type II radio bursts observed by e-CALLISTO and then analyze their space weather implication in terms of the ionospheric total electron content (TEC) enhancement.

https://doi.org/10.5194/egusphere-2023-201
Preprint. Discussion started: 16 February 2023

2 Observation

2.1 Type II Radio bursts observation

The radio data presented in the current work were observed by e-CALLISTO from May 2021 to December 2022 of solar cycle 25. We started with the list of radio events observed by this instrument hosted at the website (https://e-callisto.org) and selected 31 well separated type II radio bursts whose morphologies are clear, examined their association with the current solar phenomena to give insights on the status of the ascending phase of the solar cycle 25. Each selected type II radio burst was attributed to associated coronal mass ejection (CME) and the onset of solar flare was to analyze the implications of space weather in terms of TEC. The CME parameters were taken from the Large Angle and Spectrometric COronagraph (LASCO C2) on board the Solar and Heliospheric Observatory (SOHO, Brueckner et al., 1995) catalog updated to 2022 December 30.

2.2 Derivation of shock characteristic parameters

We start this analysis by measuring the instantaneous bandwidth (BDW) of type II radio bursts

$$BDW = \frac{f_u - f_l}{f_l} \tag{1}$$

where $\mathrm{f_u}$ and $\mathrm{f_l}$ denote the upper and lower frequencies, respectively of the fundamental emission band. Figure 1 shows an example of type II radio burst from 03:28:25 UT to 03:32:30 UT on April 17, 2022 for which $\mathrm{f_u}$ and $\mathrm{f_l}$ are indicated. This bursts is associated with a X1.1 flare that started at 03:17 UT and stopped at 03:51 UT from NOAA active region 12994. The values of BDW were used to estimate the density jump across the shock (e.g., Vršnak et al., 2001, 2002; Cho et al., 2007; Nedal et al., 2019), χ via the relation

$$\chi = (BDW + 1)^2 \tag{2}$$

By assuming low plasma ratio ($\beta \rightarrow 0$) for a perpendicular shock in the corona (Vršnak et al., 2001, 2002), the density jump allows one to compute the Alfvén Mach number (M) using Rankine-Hugoniot approximation

$$M_A = \sqrt{\frac{\chi(\chi+5)}{2(4-\chi)}} \tag{3}$$

It has been shown that the rate of change of the frequency of metric type II radio bursts is related to the shock speed and the electron density gradient in the solar corona (e.g., Gopalswamy, 2011; Vemareddy et al., 2022) through the relation

$$V_s = -\frac{2r}{\alpha}\left(\frac{1}{f}\right)\left(\frac{df}{dt}\right) \tag{4}$$

where r is the shock formation height, α is a fitted empirical index of density variation over the heliocentric distance, f is the starting frequency, and $\frac{df}{dt}$ is the frequency drift rate. The electron density decreases with heliocentric distance from the Sun, according to the power-law: $\mathrm{n_e(r)} \propto \mathrm{r}^{-\alpha}$. Three different density models given by Newkirk (1967), Saito et al. (1977) and Leblanc et al. (1998) describe the variation of the electron density in the corona and interplanetary medium. With these models,

https://doi.org/10.5194/egusphere-2023-201
Preprint. Discussion started: 16 February 2023

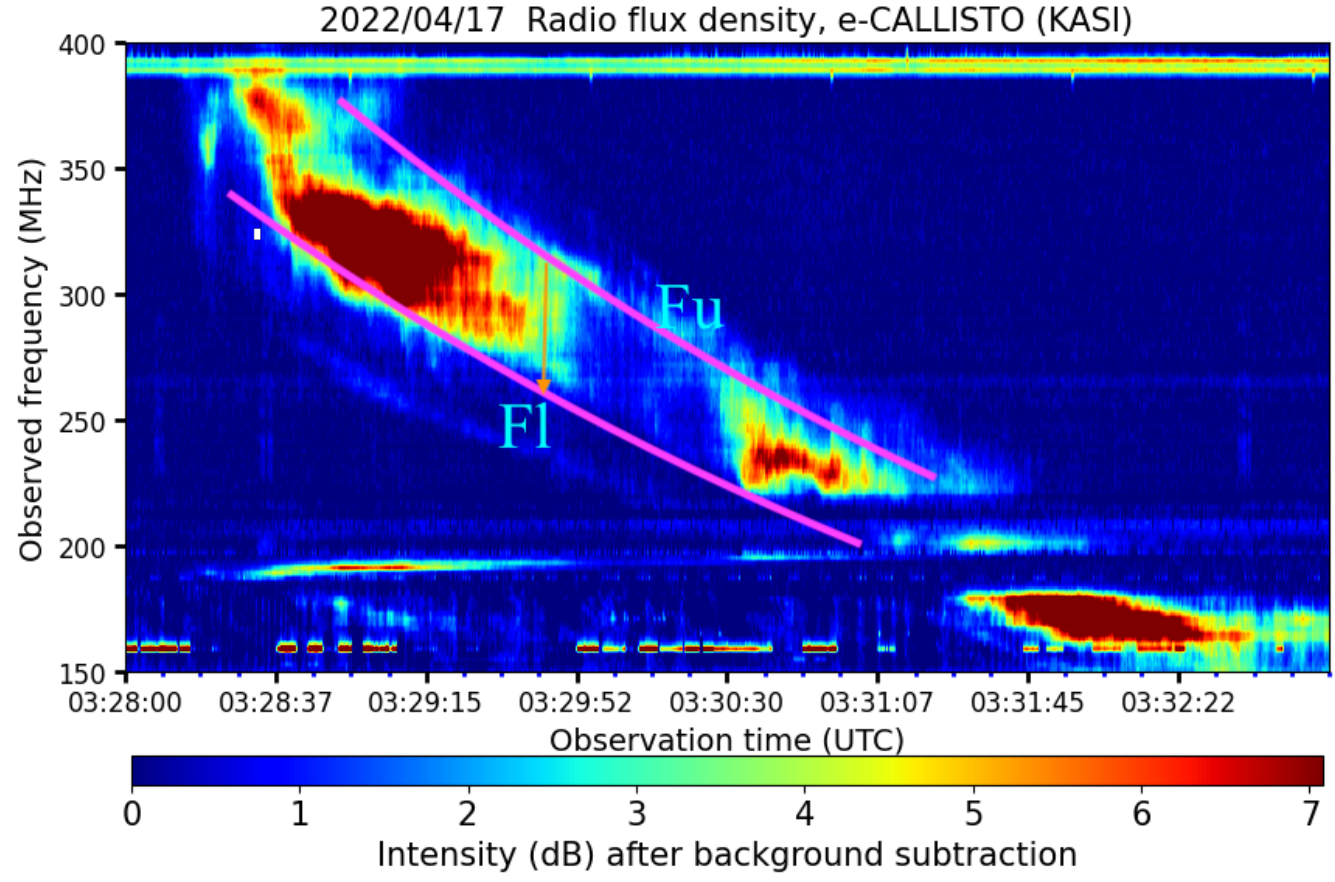

Figure 1. Type II radio burst from 03:28:25 UT to 03:32:30 UT observed by Korean Astronomy and Space science Institute (KASI) on April 17, 2022. F_u and F_l denote the upper and lower frequencies of the fundamental band of the type II radio emission.

it has been observed that within $1-3$ solar radii $(R_\odot)$, the electron density is directly proportional to r^{-6} in the corona and directly proportional to r^{-2} beyond few tens of solar radii. Because the type II radio observed all have occurred in the range of $\sim 1-2\ R_\odot$, α is chosen to be 6.13 (Gopalswamy, 2011). The Alfvén velocity is directly related to the shock speed as

$$V_A = \frac{V_s}{M_A} \tag{5}$$

In the region surrounding a CME, the ambient magnetic field strength (B) of the plasma can be estimated using the relation (Vršnak et al., 2002; Cho et al., 2007; Lata Soni et al., 2021)

$$B = 5.1 \times 10^{-5} \times f_l \times V_A \tag{6}$$

GPS data from ground-based GPS receiver stations in different locations of the globe were used to analyze the ionospheric total electron content (TEC). These include the African Geodetic Reference Frame (AFREF) database (http://afrefdata.org/)

https://doi.org/10.5194/egusphere-2023-201
Preprint. Discussion started: 16 February 2023

and UNAVCO Archive of GNSS Data (https://www.unavco.org/). GPS data were acquired in Receiver Independent Exchange format and converted to TEC information using the most recent version of the GPS-TEC analysis application software (Version 3.0) developed by Seemala and Valladares (2011), which can be downloaded from the website https://seemala. blogspot.com. The GPS-TEC programme reads raw GPS data from Receiver Independent Exchange files and calculates phase and code TEC values for the epochs, as well as corresponding elevation and azimuth angles of the satellites.

3 Results and Discussions

3.1 Comparison and analysis

During the ascending phase of the solar cycle 25, the e-CALLISTO network observed a series of solar radio bursts in the range from 10 MHz to 870 MHz. With the interest of space weather diagnostics, 31 well separated type II radio bursts observed by this network are presented in this study. Using the radio parameters such as bandwidth, drift rate and starting frequency, the shock characteristics from each radio event have been estimated. Table 1 illustrates each type II radio burst selected and associated CME , GOES soft X-ray flares as well as shock characteristics. The first column of this table is the numbering index of the events, the next four columns are the date of the radio events in the format dd/mm/yyyy hh:mm, their starting frequencies, f (MHz), their drift rates (MHz/s) and their shock formation heights ($R_{\odot}$) estimated using the relation $f(r) = 307.87r^{-3.78} - 0.14$ (Gopalswamy et al., 2013). Columns 6 to 9 are the GOES soft X-ray flares parameters (start, class, NOAA region and location) followed by two columns of CME that present the CME onset and speed, respectively. Columns 12 to 15 present the shock characteristics (density jumps, Mach numbers, shock and Alfvén velocities, respectively) while the last column of this table presents the estimated ambient magnetic field strength, B (Gauss). There is a strong correlation (CC=0.905) between the drift rates and starting frequencies of the type II radio bursts (Figure 2) which are the key parameters to estimate the shock speeds from the dynamic spectra. Such correlation agrees well with the previous studies (e.g., Vršnak et al., 2002; Umuhire et al., 2021). From Table 1, it is clearly observed that 4/31 radio events are not associated with any solar flare because they originate from farside on the solar surface but the shocks generating these bursts were excited by associated CMEs. It is also noticed that 18/27 are connected with intense GOES X-ray flares (M & X classes), which is compatible with their speeds as well as estimated shock speeds. We derived the shock and Alfvén speeds of these type II radio bursts in the order of 504 - 1301 kms^{-1} and 368 - 837 kms^{-1}, respectively at heliocentric distance $\sim 1-2\ R_{\odot}$ with the exception of one event having shock and Alfvén speeds of 2426 and 1344 km/s due to its higher drift rate associated to its high starting frequency (Umuhire et al., 2021). Comparatively, values are consistent with the measurements reported by Cunha-Silva et al. (2015); Minta et al. (2023) about 590 - 810 kms^{-1} and 250 - 550 kms^{-1}, respectively at $\sim 1.2-1.8\ R_{\odot}$. The Alfvén speeds from the current work are also in agreement with the range of the Alfvén speeds of 140 – 460 kms^{-1} over 1.2 – 1.5 $\mathrm{R}_{\odot}$ and 259 – 982 kms^{-1} over 3 - 15 $\mathrm{R}_{\odot}$ given in Gopalswamy et al. (2011) and in Kim et al. (2012), respectively. Figure 3 presents the number of type II radio events observed and associated shock speeds derived from dynamic spectra as well as the speeds of associated CMEs recorded by the LASCO. Table 1 observations show that there are estimated shock speeds that are faster than CME speeds from LASCO FOV and vice versa. However, the mean and median shock speeds estimated from the dynamic spectra are faster than those

https://doi.org/10.5194/egusphere-2023-201
Preprint. Discussion started: 16 February 2023

Table 1. Type II radio bursts observed by e-CALLISTO during the ascending phase of solar cycle 25 and their associated CMEs, GOES soft-Xray flares and estimated shock characteristics.

No	Type II burst event				Soft X-ray flare				CME		Shock characteristics				B-field
	Date (UT)	f (MHz)	Drift rate ($MHzs^{-1}$)	height $R_\odot$	Start (UT)	Class	NOAA	Location	Onset (UT)	Speed (kms^{-1})	χ	M	V_s (kms^{-1})	V_A (kms^{-1})	G
1	22/05/2021 02:57	86	- 0.13	1.4	02:47	C6.1	12824	N18E25	.....	.....	1.6	1.5	752	504	1.5
2	23/06/2021 07:05	73	-0.10	1.5	06:43	C3.4	12833	N14E89	07:24	491	1.5	1.4	668	464	1.2
3	25/07/2021 04:54	64	-0.11	1.5	.....	....	F. S.	.....	05:48	299	1.3	1.2	785	637	1.6
4	28/08/2021 05:10	64	-0.15	1.5	05:01	C7.0	12860	S31E06	.....	.....	1.7	1.6	1170	728	1.6
5	09/10/2021 06:34	75	- 0.12	1.5	06:19	M1.6	12882	N18E06	07:00	712	1.6	1.5	790	533	1.4
6	09/10/2021 06:49	31	- 0.04	1.9	06:19	M1.6	12882	N18E06	07:00	712	1.3	1.3	706	561	0.7
7	20/12/2021 11:27	87	- 0.16	1.4	11:12	M1.8	12908	S20W01	12:23	359	1.7	1.6	860	549	1.7
8	12/01/2022 04:28	69	- 0.17	1.5	.....	....	F. S.	.....	04:36	1586	1.8	1.7	1264	742	1.7
9	12/02/2022 08:33	173	- 0.36	1.2	08:25	M1.4	12939	S17W82	08:12	280	1.3	1.2	792	659	4.1
10	02/03/2022 17:42	67	- 0.11	1.5	17:31	M2.0	12958	N15E29	18:24	442	1.9	1.7	924	532	1.1
11	14/03/2022 17:20	98	- 0.20	1.4	17:13	B8.5	12964	S30W86	17:36	740	1.9	1.7	1373	786	1.8
12	25/03/2022 05:15	66	- 0.12	1.5	05:02	M1.4	12974	S18E37	05:36	495	1.5	1.4	801	590	1.5
13	28/03/2022 11:23	242	- 0.97	1.1	10:58	M4.0	12975	N18W04	11:53	702	1.9	1.8	2426	1344	6.7
14	30/03/2022 17:33	72	- 0.12	1.5	17:21	X1.3	12975	N13W31	18:00	641	1.9	1.8	1213	686	1.1
15	31/03/2022 18:34	67	- 0.15	1.5	18:17	M9.6	12975	N12W47	18:53	625	2.0	1.8	1284	705	1.5
16	02/04/2022 13:24	71	- 0.14	1.5	12:56.	M3.9	12975	N12W68	13:23	1433	1.9	1.8	1012	576	1.4
17	17/04/2022 03:28	382	- 0.83	0.9	03:17	X1.1	12994	N12E88	03:36	895	1.2	1.2	828	711	7.8
18	21/04/2022 02:00	85	-0.15	1.4	01:47	M9.6	12993	N22E23	02:24	357	1.7	1.5	1090	709	1.6
19	21/04/2022 22:47	69	-0.11	1.5	22:39	C1.6	12993	N12E25	23:12	405	1.4	1.3	791	591	1.4
20	30/04/2022 13:46	83	-0.13	1.4	13:37	X1.1	12994	N16W88	14:00	498	1.7	1.5	936	610	1.4
21	30/04/2022 19:50	80	-0.12	1.4	19:42	M1.9	12994	N16W88	20:00	648	1.7	1.6	855	543	1.3
22	04/07/2022 13:35	69	-0.13	1.5	12:23	C5.1	13050	N17E36	14:00	352	1.7	1.6	918	581	1.4
23	05/07/2022 04:16	69	-0.10	1.5	03:59	C9.8	13045	S20W18	04:36	747	1.6	1.5	761	512	1.2
24	14/08/2022 12:05	70	-0.08	1.5	11:50	C2.4	13076	N21W14	12:48	481	1.4	1.3	512	402	1.1
25	18/08/2022 12:12	62	-0.16	1.6	.....	....	F. S.	.....	11:00	1327	1.7	1.6	1301	837	1.9
26	19/08/2022 04:35	81	-0.10	1.4	04:14	M1.6	13078	S27W48	04:49	832	1.3	1.3	504	420	1.4
27	23/09/2022 18:02	67	-0.13	1.5	17:48	M1.7	13110	N16E84	18:12	1644	2.0	1.8	1107	601	1.3
28	29/09/2022 12:06	80	-0.10	1.4	11:50	C5.7	.....	N26E86	12:24	321	1.5	1.4	672	473	1.2
29	09/11/2022 20:03	89	-0.11	1.4	.....	....	F. S.	.....	20:36	371	1.5	1.4	618	435	1.3
30	03/12/2022 17:44	84	-0.13	1.4	17:36	M1.2	13157	N14E89	18:12	322	1.8	1.8	857	518	1.3
31	14/12/2022 08:30	160	-0.22	1.2	08:24	M1.1	13162	S16W89	08:36	385	1.9	1.8	657	368	1.7

estimated from the LASCO FOV. Figure 3 (a) shows mean and median speeds of 893 and 841 km/s, respectively, while Figure 3 (b) shows mean and median speeds of 658 and 498 km/s. Solar radio type II bursts associated with slow CMEs are thought to be generated by from the non-thermal electrons accelerated by a moving magnetic reconnection when slow CMEs interact with the background magnetized coronal plasma (Tan et al., 2019). Furthermore, a recent study confirmed that observing a type II radio burst is evidence of shock acceleration in the solar corona (Chernov and Fomichev, 2021).

The Alfvén Mach numbers in the range $\sim 1.2-1.8$ at $\sim 1-2$ $R_\odot$ are consistent with the measurements of about 1.1 - 1.9 at $\sim 1.3-2.5$ R$\odot$ reported by Vršnak et al. (2002) and that of Cunha-Silva et al. (2015) in the order of 1.4 to 1.7 at $\sim 1.2-1.8$ $R_\odot$.

https://doi.org/10.5194/egusphere-2023-201
Preprint. Discussion started: 16 February 2023

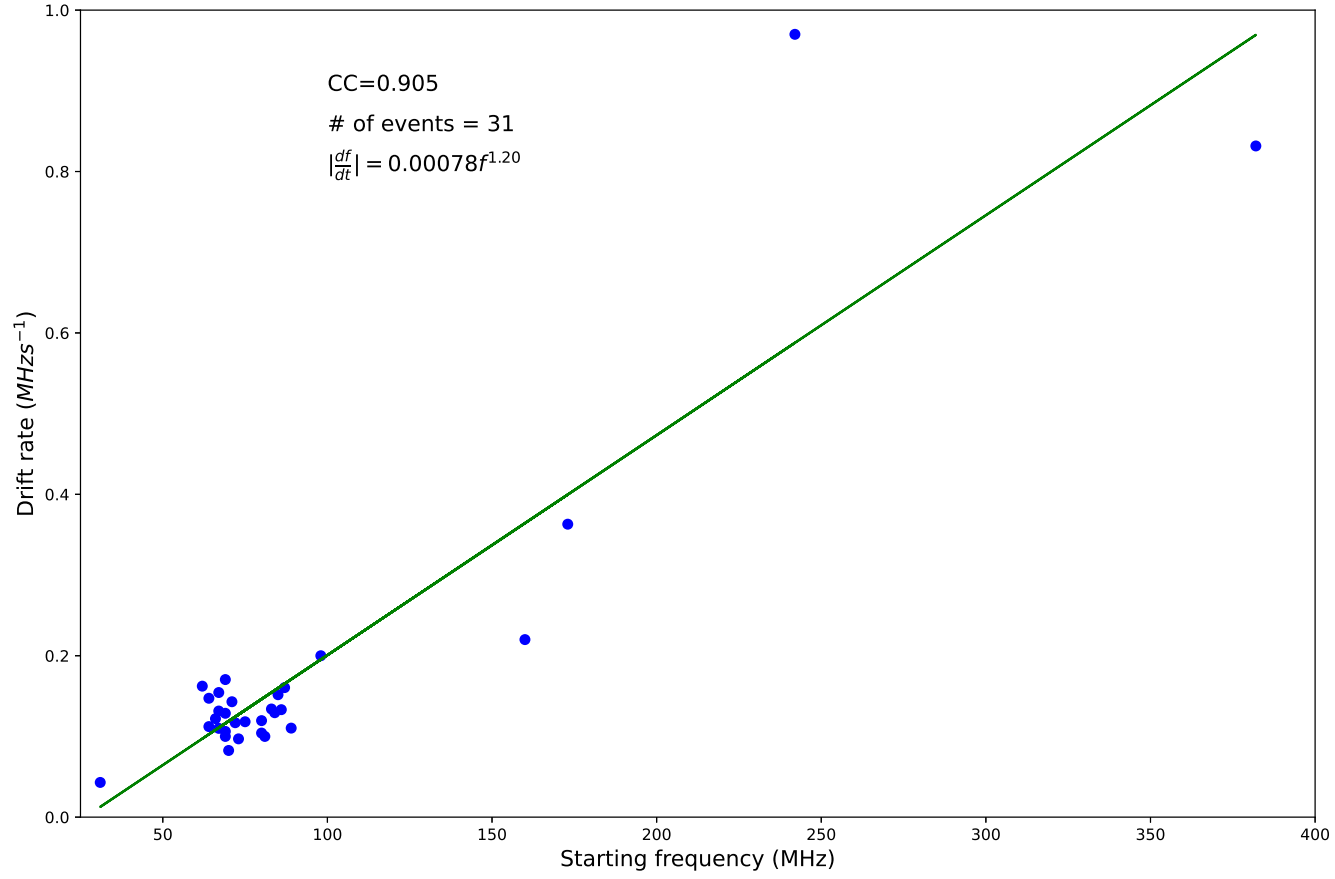

Figure 2. Scatter plot between the absolute drift rates ($|\frac{df}{dt}|$) and the starting frequency f_s for all the 31 metric type II radio bursts. The power-law least squares fits and the corresponding correlation coefficient Cc are shown.

The magnetic field strength is an important parameter that influences the dynamical eruption of CMEs in the solar atmosphere (e.g., Sasikumar Raja et al., 2014; Carley et al., 2017). High-starting type II radio bursts are associated with coronal shocks that are closer to the solar surface. As a result, high magnetic field values are expected. Figure 4 demonstrates the variation of the magnetic field strength estimated in this study (Equation 6) relative to the quiet Sun magnetic field model $B(r) = \frac{a}{r^2}$ with $a = 2.2$ and Dulk and McLean (1978) empirical model for the magnetic field above active region $B(r) = 0.5\,(r-1)^{-1.5}$. The magnetic field has been calculated in the range $0.6 < B < 8\ G$ at $\sim 1-2\ \mathrm{R}_\odot$, which shows excellent consistency and is fitted with a single power-law distribution of the type $B(r) = 6.56r^{-3.92}\ G$ as represented by the black dotted curved of Figure 4. However, Rankine - Hugoniot jump relation has been used by a number of researchers to derive shock parameters. For example, with this technique Smerd et al. (1974, 1975) found $1.2 \leq \mathrm{M_A} \leq 1.7$ and $0.3 \leq \mathrm{B} \leq 4$ G. The same technique was applied by Vršnak et al. (2002) who reported a magnetic field strength in the range 1 - 8 G at heliocentric distance of ~ 1.6 $R_\odot$. A field strength of 6 - 5 G at $\sim 1.5-1.77\ \mathrm{R}_\odot$ is reported by (Ramesh et al., 2010). Dulk and McLean (1978); Sasikumar

https://doi.org/10.5194/egusphere-2023-201
Preprint. Discussion started: 16 February 2023

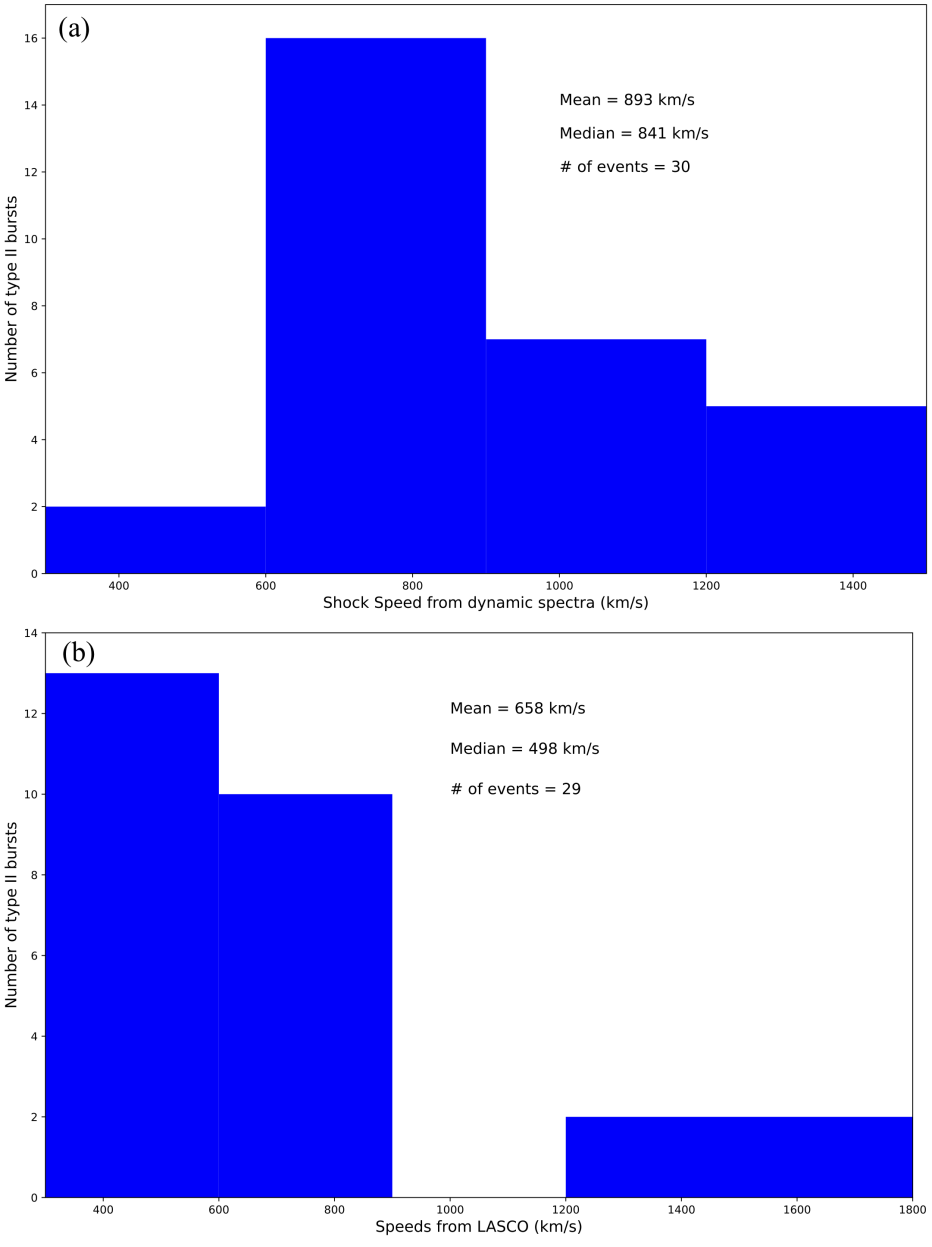

Figure 3. (a) Distribution of CMEs speed from the dynamic spectra with the observed average and median are 893 and 841 km/s. (b) Distribution of CME speeds from LASCO FOV with average and median of 658 and 498 km/s, respectively. The average and median speeds are higher than in LASCO and are attributed to the radio source, which propagates at faster speeds due to the interaction of slow CMEs with background magnetized coronal plasma (Tan et al., 2019).

https://doi.org/10.5194/egusphere-2023-201
Preprint. Discussion started: 16 February 2023

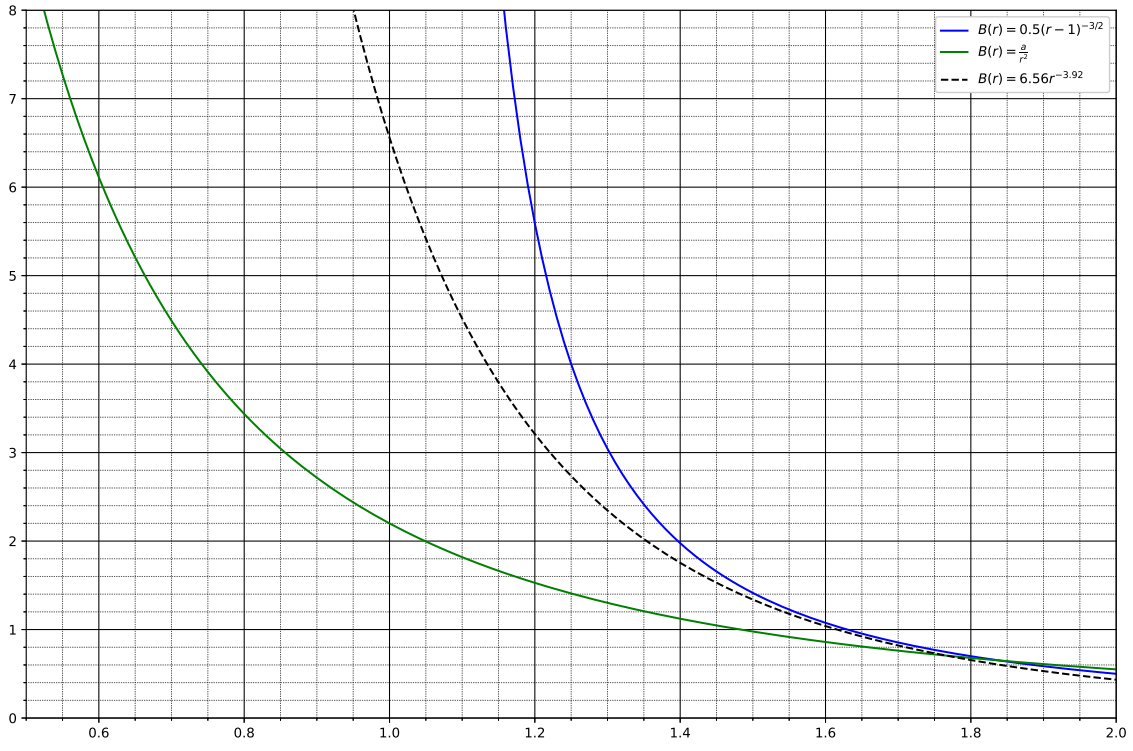

Figure 4. Comparison of the magnetic field strength from the current study, the quiet Sun magnetic field model and the empirical magnetic field relation (Dulk and McLean, 1978). The magnetic values estimated are all above the quiet Sun magnetic model and the pattern is close to the empirical mode which confirms that the Sun was awake.

Raja et al. (2022) have given a detailed review on solar coronal magnetic fields measured using different techniques and at different wavelengths of the electromagnetic spectrum. A recent work has reported that two necessary conditions for type II radio emissions: (i) relatively intense shock waves (the Mach number should exceed a certain value $\mathrm{M_{cr}}$) and (ii) perpendicular shock waves are required (Chernov and Fomichev, 2021). Our values of Mach numbers $1.2 \leq \mathrm{M_A} \leq 1.8$ agrees well with these conditions.

3.2 Associated Space weather implication

The ascending phase of solar cycle 25 is characterized by high solar activity than expected (SW, 2022). This is indicated by a number of space weather events that have been registered by SWPC. Tan (2011) and Sarp et al. (2018) show that solar cycle 25 is more active than the previous cycle and is more consistent with actual observations as predicted. Furthermore, Du (2020) estimated that the maximum peak of cycle 25 would be 30% stronger than that of cycle 24. These indicate that the activity would be high, and we use this advantage to track the intensity of early space weather events in the current cycle. Illustrative

https://doi.org/10.5194/egusphere-2023-201
Preprint. Discussion started: 16 February 2023

examples of type II radio events are selected based on their occurrence and are used to highlight some space weather hazards recognized.

3.2.1 October 9, 2021 event

Type II radio bursts on 2021 October 9, was recorded among other spectrometers of e-CALLISTO by Astronomical Society of South Australia (Australia-ASSA): the first type II burst is recorded in the time range of 06:34 UT to 06:42 UT overlapped by a type IV radio burst from 06:37 UT to 06:46 UT. Another type II radio burst is registered from 06:49 UT to 06:55 UT with band-splitting feature as it is displayed in the top panel of Figure 5. All of these events are associated by GOES soft X-ray flare of M1.6 class that started at 06:19 UT, peaked at 06:38 UT and stopped at 06:53 UT from NOAA 12882 explosion. They are also associated with a halo CME observed by LASCO C2 coronagraph with onset at 07:00 UT with a speed of 712 kms^{-1}. This CME has reached near Earth on 2021 October 12 and caused a geomagnetic storm at 14:30 UT with Dst = -65 nT. It is observed that few minutes after the first type II has started, an enhancement of protons took place as an effect of radio blackout depicted in bottom of Figure 5. It is noted that the flare has no direct interaction with the magnetosphere but its radiation agents (X-rays, UV, EUV) perturb the ionosphere by increasing the ionization which in turn causes the signal delay in Global Navigation Satellite Systems (GNSS) (e.g., Amory-Mazaudier et al., 2017). Table 2 lists the codes, country, geographic and geomagnetic coordinates of some GNSS stations used in the current study for a reference. Figures 6 (a) and (b) show the

Table 2. Geographic and Geometric coordinates of some GNSS stations used for this study

		Geographic coordinates		Geomagnetic Coordinates		
Code	Country	Lat(deg)	Long (deg)	Lat(deg)	Long (deg)	Altitude (m)
abpo	Madagascar	-19.018	47.229	-23.30	116.73	1552.992
bogt	Colombia	4.640	74.081	13.87	-1.46	2576.778
falk	Falkland Island	-51.694	-57.874	-52.50	12.44	50.841
iisc	India	13.021	77.570	4.86	150.94	843.713
mbar	Uganda	-0.601	30.738	-2.73	103.13	1337.653

variations in ionospheric total electron content (TEC) after flares and radio bursts from two affected stations, one in Africa and the other from Asia, the regions affected during the radio blackout. Figure 6 (a) shows a dramatic increase and decrease in TEC, with peaks at around 12:00 UT of 21 TECU Units (TECU, $1\ TECU = 10^{16}\ electrons/m^2$), 25.5 TECU, and 18 TECU for Day of the Year (DOY) = 281, 282, and 283, respectively. Similarly, Figure 6 (a) depicts an instantaneous increase in TEC with peaks of 34 TECU, 40 TECU, and 44.5 TECU at around 12:00 UT. The Kp indices for these three days are 2, 2, and 4, indicating that 2021 October 10 (DOY=283) was more magnetically active than the previous two days. The decrease in TEC at Antananarivo station on this day indicates a negative ionospheric storm, whereas the increase in TEC at Bangalore station indicates a positive ionospheric storm.

https://doi.org/10.5194/egusphere-2023-201
Preprint. Discussion started: 16 February 2023

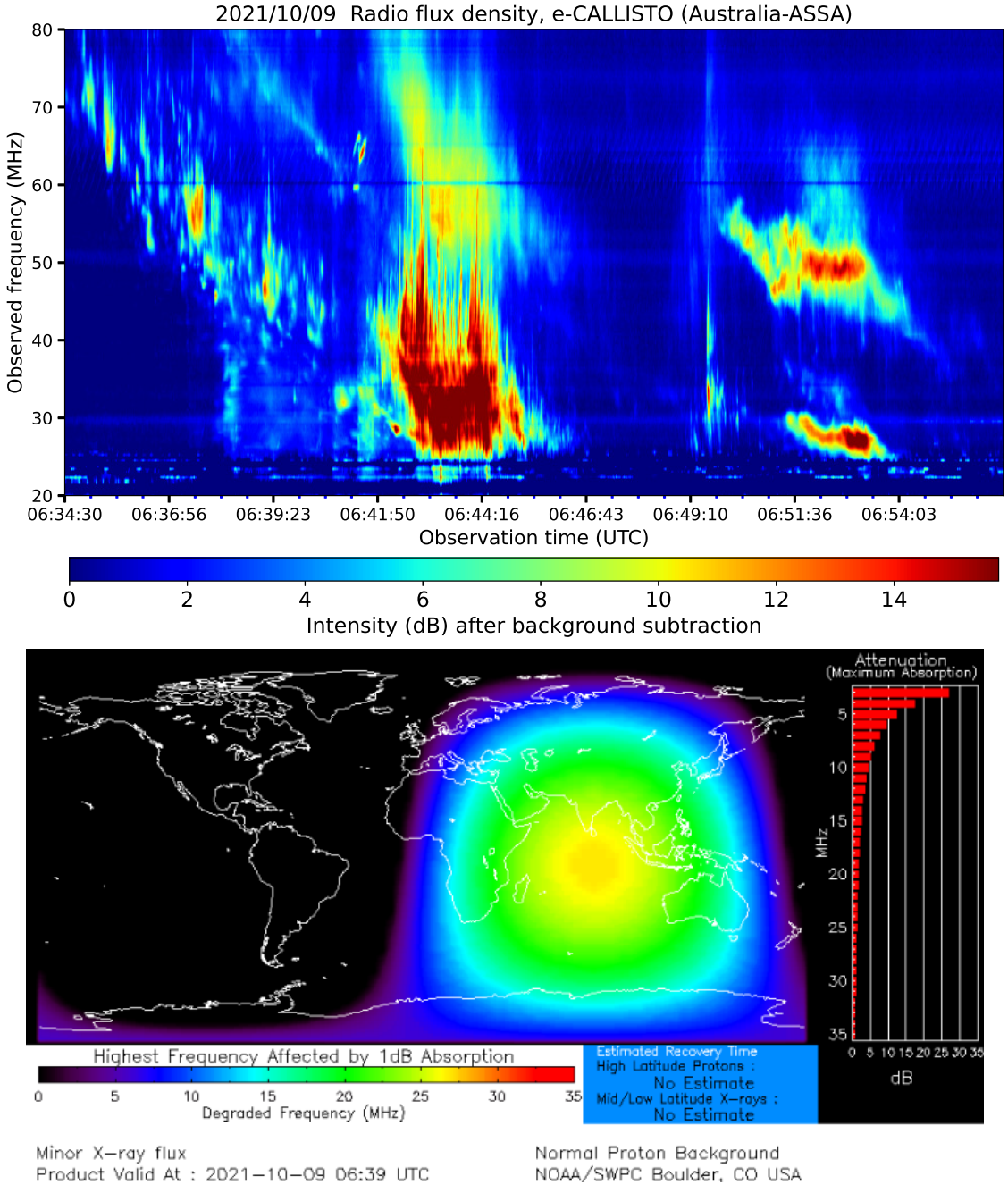

Figure 5. The top panel shows type II radio emissions that are observed on 2021 October 9. Lower panel shows a minor radio blackout that occurred over Africa, the Indian Ocean, Europe , Australia and Asia on 2021 October 9 due to the enhancement of X-ray flux and UV radiation at the Earth. Credited to the SWPC.

https://doi.org/10.5194/egusphere-2023-201
Preprint. Discussion started: 16 February 2023

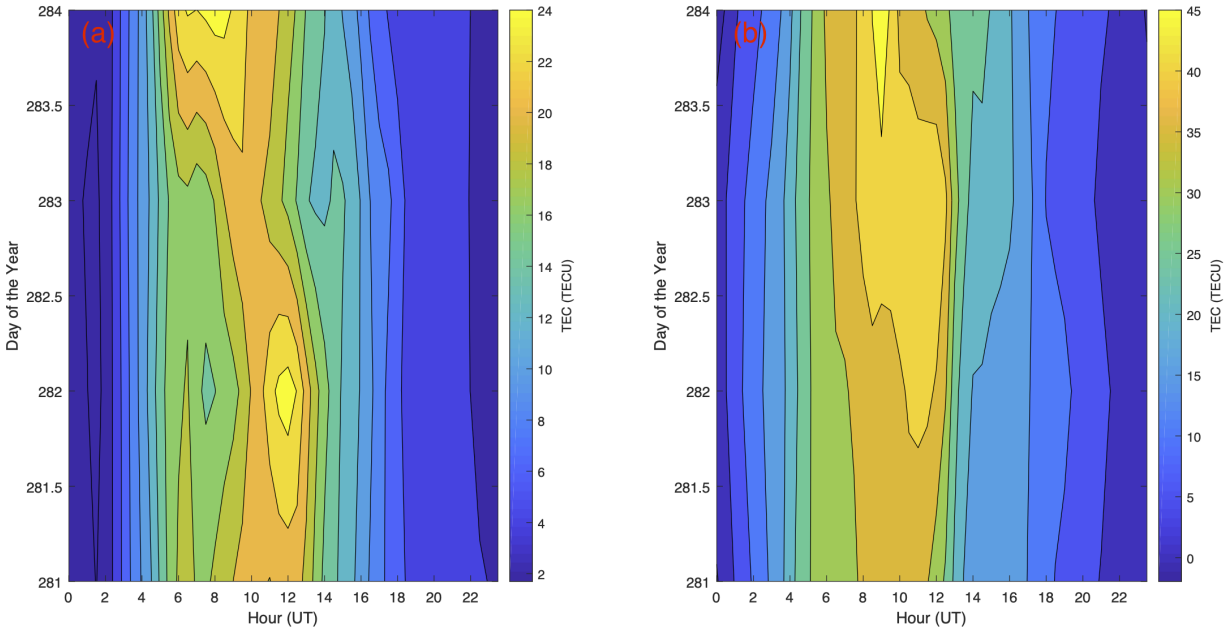

Figure 6. Three-day contour plots of (a) TEC over Antananarivo (Madagascar) and (b) TEC over Bangalore (India) between 2021 October 8 - 11 (DOY 281 - 284) in comparison to 2021 October 9 (DOY=282) beginning at sim06:20 UT. The maximum TEC over Antananarivo on each day is 21 TECU, 25.5 TECU, and 18 TECU at around 12:00 UT for DOY= 281, 282, and 283, respectively. These are 34, 40, and 44.5 TECU at Bangalore station.

3.2.2 March 24 - April 3, 2022

The solar activity is seen to be high during March 2022. This is due to a number of solar events observed and recorded during this month. In fact, seven type II radio events were recorded in March 2022. Five of the seven events are in close proximity and are used to discuss the ionospheric TEC variation this month. Figure 7 presents a type II radio burst observed by e-CALLISTO network at Arecibo Observatory in Puerto Rico, USA from 11:23:12 UT to 11:28:37 UT on March 28, 2022 with 87 - 32 MHz frequency range. This burst is overlapped by a type IV radio burst that occurred from 12:26 UT to 11:35 UT. These bursts are associated with GOES soft X-ray flare M4.0 that started at 10:58 UT, peaked at 11:29 UT and stopped at 11:45 UT from NOAA 12975. This eruption also produced a tsunami in the solar atmosphere (see, https://sdo.gsfc.nasa.gov/data/dailymov/movie.php?q=20220328_1024_0193). The bursts are also associated with a partial halo CME with speed of 416 kms^{-1} and the CME was off Sun - Earth line because no geomagnetic storm is linked to it. However, the flare and the tsunami accelerated protons that hit the Earth's magnetosphere and caused a minor radiation storm. The enhancement of proton events is revealed by the radio blackout that cover the whole African continent (see top panel of Figure 8). The lower panel of Figure 8 shows the polar cap absorption event (PCAE) that occurred after about 2:40 UT from the burst onset. This event is a signature of

https://doi.org/10.5194/egusphere-2023-201
Preprint. Discussion started: 16 February 2023

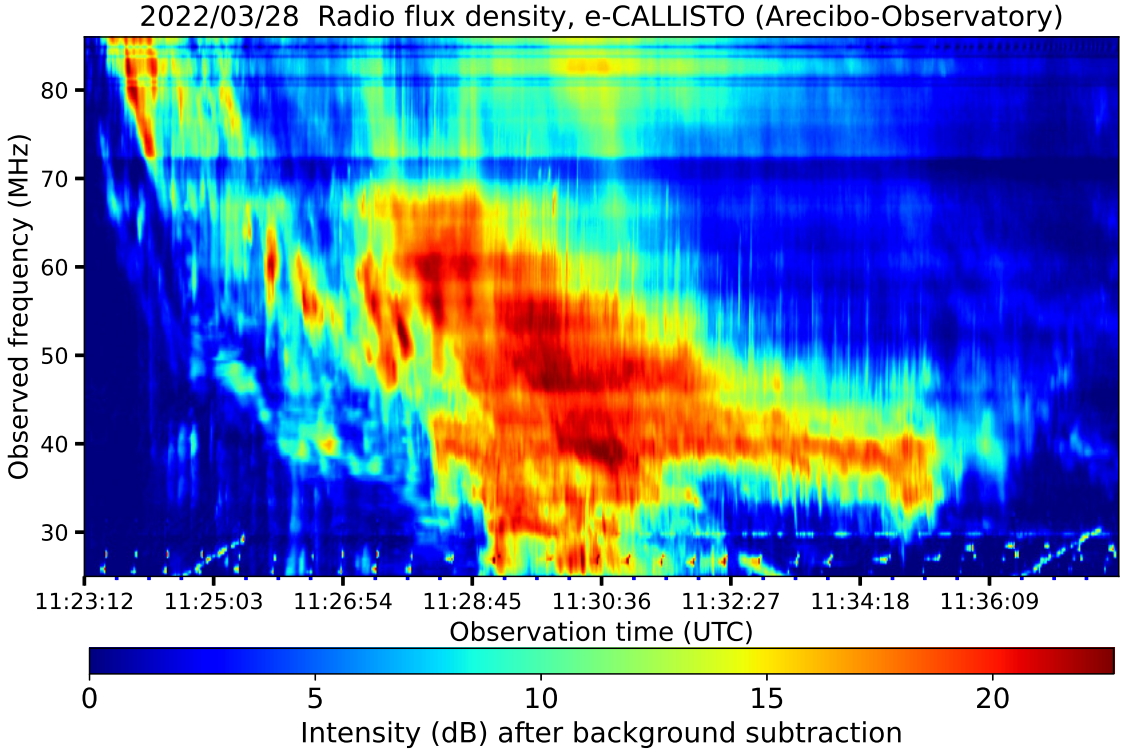

Figure 7. The type II radio emissions that are observed on March 28, 2022 from 11:23:12 UT to 11:28:37 UT followed by a type IV radio bursts from 12:26 UT to 11:35 UT.

solar energetic particle (SEP) acceleration where high frequency (HF) and very HF (VHF) are absorbed and low and very low frequencies are reflected at low altitude. Previous works showed that solar flares that cause solar proton events (SPEs) are usually accompanied by radio bursts and noise storms that disturb the ionospheric TEC (Ranta et al., 1993); and mostly observed 20 minutes to 20 hours after the solar flare (Mitra, 1974; Kavanagh et al., 2004; Perrone et al., 2004). They also showed that SPEs and PCAEs are frequent close to the maximum solar cycle (Shea and Smart, 2002), but the solar cycle 25 is far from its maximum. Thus, these observations are the evidence of high solar activity during the ascending phase of the current . It is important to note that the association of type II radio bursts with space weather drivers such as solar flares, SEPs and coronal mass ejections make them special for space weather (Kumari et al., 2019; Ndacyayisenga et al., 2021b). Furthermore, the TEC from four different stations are illustrated in Figure 9 to trace the ionospheric storm that perturbed the GNSS signals. Figure 9 (a) and (b) present two stations from Africa (Antananarivo and Mbarara stations) while Figure 9 (c) maps TEC over Bogota station (Colombia) and Figure 9 (d) depicts the TEC over Port Stanley station (Falkland Islands, south Atlantic Ocean) during March 24 - April 3, 2022 (DOY: 83 – 93). The geographic and geomagnetic coordinates of these stations are given in Table 2. Because of their geographic and geomagnetic coordinates, the first two stations provide maximum TEC between 11:00 UT and 12:00 UT, while the last two provide maximum TEC between 16:00 UT and 18:00 UT. Figure 9 (a) depicts TEC

https://doi.org/10.5194/egusphere-2023-201
Preprint. Discussion started: 16 February 2023

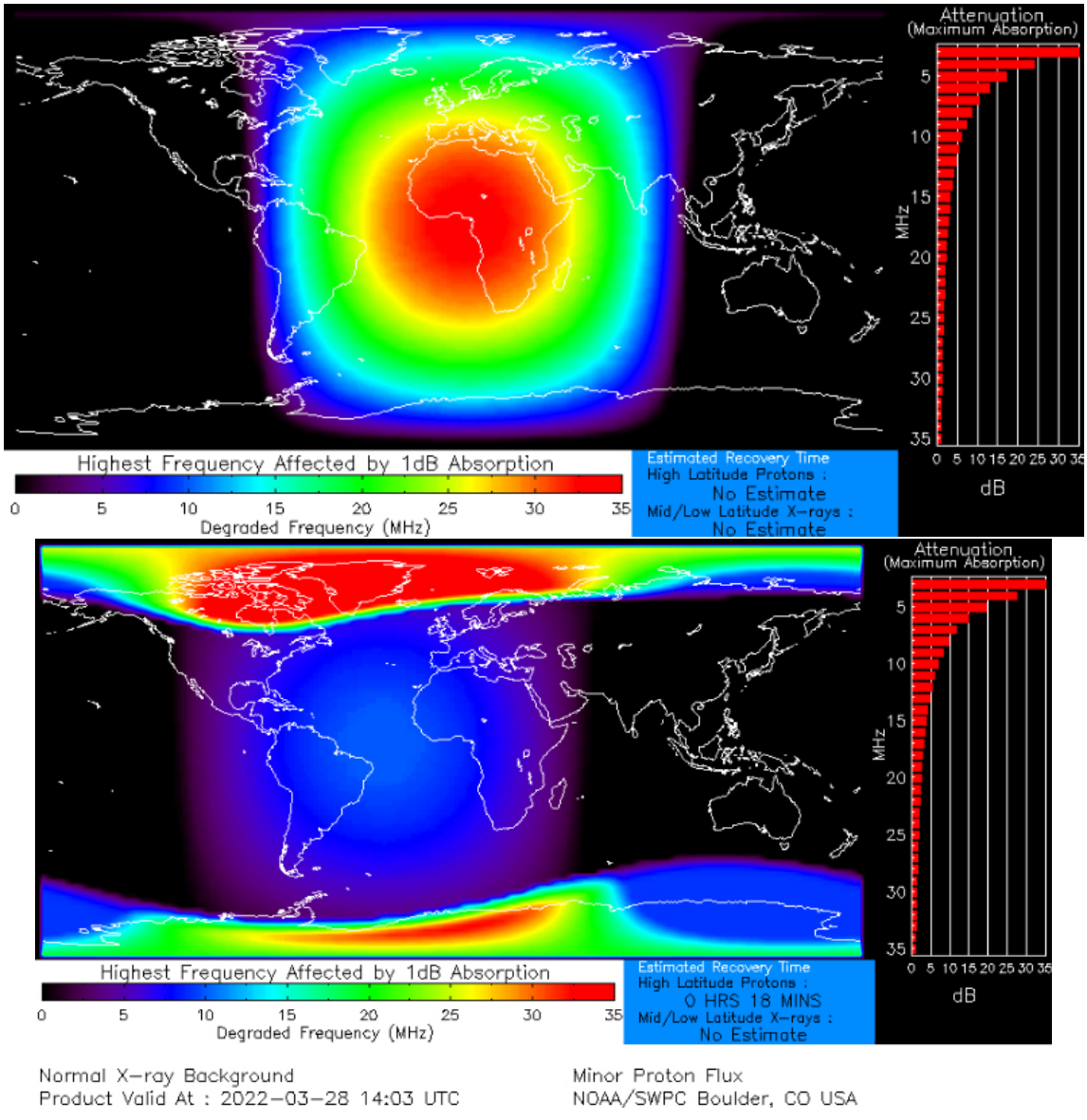

Figure 8. Top panel: The radio blackout due to proton enhancement induced by a M4.0 flare on March 28, 2022. Lower panel shows a polar cap absorption event that occurred 2:40 UT after the registration of type II on March 28, 2022 due to solar energetic particle acceleration. Credited to the SWPC.

variation at this station, with TEC peaking at 11:30 UT in the following order over the 11 days: 36, 31.5, 29, 33, 35, 42, 36, 45, 46, 30, 35, and 42, 36, 45, 46, 30, 35 TECU, respectively. These TEC fluctuations are associated with Kp indices of 3, 3, 3, 4, 2, 4, 5, 4, 5, 4, indicating that the days are nearly perturbed, which is a signature of incoming radiation agents occurring in succession on a daily basis. Figure 9 (b) illustrates the variation trend in TEC over Mbarara station from March 24 to April

https://doi.org/10.5194/egusphere-2023-201
Preprint. Discussion started: 16 February 2023

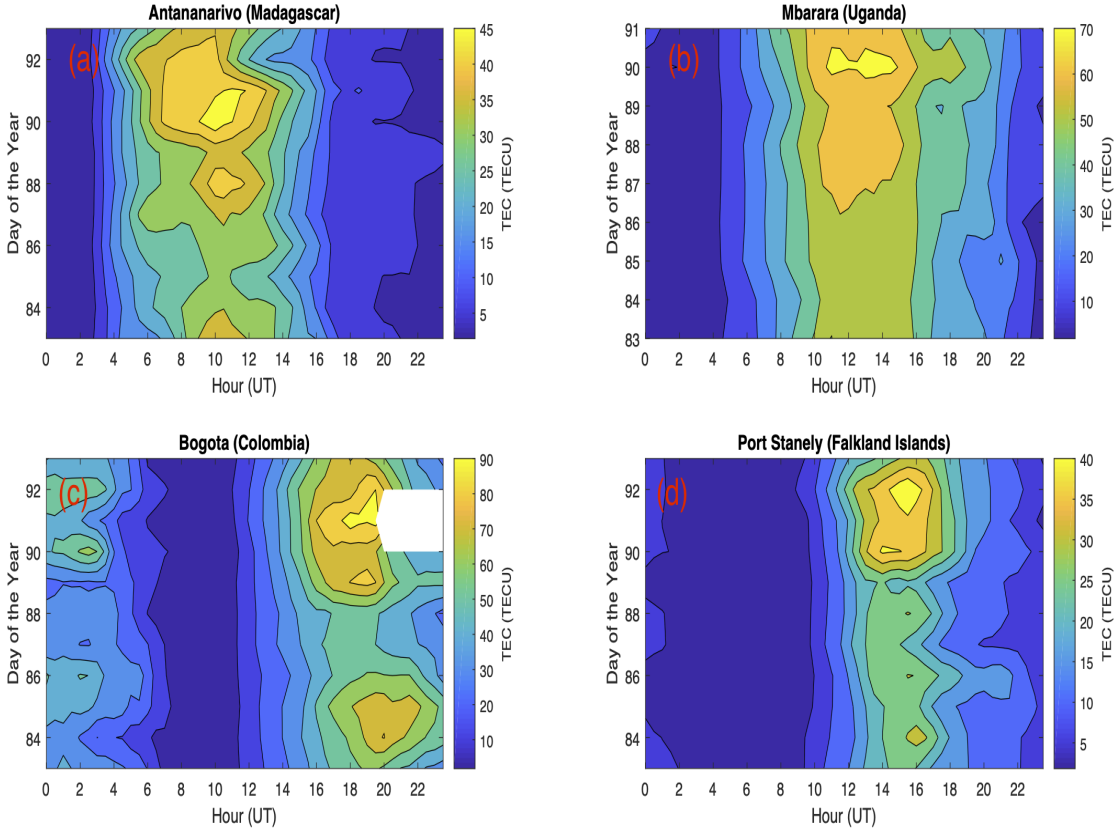

Figure 9. The eleven days contour TEC plots of DOY: 83 – 93 (March 24 - April 3, 2022) (a) 0ver Antananarivo station (Madagascar), (b) over Mbarara station (Uganda), (c) over Bogota station (Colombia) and (d) over Port Stanley station (Falkland Islands, South Atlantic ocean), respectively.

1, 2022, with peak values of TEC at 11:30 UT of 52, 55, 56, 59, 63.5, 65, 63, 72, and 69.5 TECU, respectively, corresponding to the same values of Kp indices as above. It can be seen that between 08:00 UT and 16:00 UT on March 24–26, 2022 (DOY: 83–85), the TEC is lower than on subsequent days. However, this station presented in Figure 9 (b) is located in equatorial region. The anomaly is thought to be caused by either (i) the weather condition near the Earth's equator, (ii) the effects of previous perturbations and/or (iii) equatorial ionization anomaly. On the other hand, Figure 9 (b) illustrates a prominent TEC enhancement during March 27 - April 3, 2022 (DOY: 87 – 93) covering the same time range and the TEC reached the highest value on 2022 March 31 (DOY=90). It is important to note that there is data gap at this station on 2022 April 2 which leads to plot less days of the year. Figure 9 (c) and (d) present two stations in high latitudes (North and south hemisphere, respectively). At both stations, the TEC is low between 00:00 – 12:00 UT because this time range covers the night time. A prominent TEC enhancement is observed from 15:00 UT to 21:00 UT at Bogota station (Figure 9 (c)) during March 30 - April 3, 2022 (DOY:

https://doi.org/10.5194/egusphere-2023-201
Preprint. Discussion started: 16 February 2023

89 – 93). The trend of TEC variation at this station is given by the variation of TEC maxima of the order of 56, 59, 68, 56, 52, 52, 78, 76, 92, 73, and 70 TECU at 18:00 UT, corresponding to the same Kp indices. Figure 9 (d) shows lower TEC values on March 28 (DOY=87) and March 30 (DOY=89), 2022 than the previous and following days, which is thought to be due to weather conditions over the southern Atlantic Ocean. At 16:00 UT, the variational trend of TEC maxima over this station is as follows: 26, 25, 28, 31, 31, 22, 30, 24, 39, 40, 38, and 31 TECU. These ionospheric perturbations are caused by daily strong flares, radio blackouts, and polar cap absorption events recorded between March 25 and April 3, 2022 (DOY: 84 – 93) as a result of particle enhancement. It is worth noting that agencies that rely on GPS signals located in the area depicted in Figure 9 (a) – (d) may have experienced signal delays or loss as a result of ionospheric disturbances that occurred between March 25 and April 3, 2022. (DOY: 84 – 93). Smith et al. (2017) investigated global auroral ovals using magnetic data from near-Earth orbit satellites. Their investigation is limited to auroral electrojet currents for $Kp \leq 4$, and they propose (in figure 7) that increasing Kp by 2 results in a roughly doubling of auroral electrojet current strength for $0 \leq K_p \leq 4$. It is clear from the examples above that type II radio bursts can be used as a warning of impending space weather hazards. Furthermore, 15/31 reported events are associated with immediate space weather impacts because they are associated with radio blackouts or polar cap absorption events. Only 7 of the 31 type II radio bursts studied, on the other hand, are not a potential event to disrupt space weather because they are not associated with a CME or have an immediate space weather impact, whereas the rest can be used to track geomagnetic storms within the next five days from the onset of associated CMEs. Solar radio bursts are among the earliest observed signatures of erupting events in the solar corona (Salmane et al., 2018; Ndacyayisenga et al., 2021a).

4 Summary and conclusion

In this study, we report on an analysis of 31 well separated type II radio bursts observed by e-CALLISTO network from May 2021 to December 2022. The parameters of type II radio bursts, such as bandwidth, drift rates and starting frequency are used to derive the corresponding shock parameters: the shock speed, Alfvén speed, Mach number and magnetic field strength. The shock and Alfvén speeds are estimated in the range of 504 - 1301 kms^{-1} and 368 - 837 kms^{-1}, respectively at heliocentric distance $\sim 1-2\ \mathrm{R}_{\odot}$. The range of measurements that is consistent with the earlier works including the Alfvén speed with 550 - 400 kms^{-1} given in Cho et al. (2007) at $\sim 1.6-2.1\ \mathrm{R}_{\odot}$. The Alfvén speed of the order of 140 kms^{-1} to 460 kms^{-1} at heliocentric distance $\sim 1.2-1.5\ \mathrm{R}_{\odot}$ reported in Gopalswamy et al. (2011), while Kim et al. (2012) inferred Alfvén speed in the range of 259 - 982 kms^{-1} over 3 - 15 $\mathrm{R}_{\odot}$. The shock speed estimated agrees well with the works of Cunha-Silva et al. (2015) and Minta et al. (2023) who found shock speed of the order of 200 kms^{-1} to 810 kms^{-1}. Using Rankine-Hugoniot approximation, the Mach number of the order of 1.2 to 1.8 is obtained and the magnetic field strength in the range of $\sim 7.8-0.7\ G$ which is fitted with a single power-law s $B(r) = 6.56r^{-3.92}\ G$ at the same heliocentric distance. The range of Mach number is in good agreement with the range of Mach number of $1.59 < \mathrm{M_A} < 2.53$ reported by Mann et al. (2022) and $\mathrm{M_A} \geq 1.5$ by Su et al. (2022). Our magnetic field strength estimate of the order $\sim 7.8-0.7\ G$ at $\sim 1-2\ \mathrm{R}_{\odot}$ is well consistent with the work of Vršnak et al. (2002) who reported the magnetic field strength of 1 - 8 G at $\sim 1.6\ \mathrm{R}\odot$ and also with 6 - 5 G at $\sim 1.5-1.7\ \mathrm{R}\odot$ found in Ramesh et al. (2010). The current work finds that 15/31 type II radio events analyzed

https://doi.org/10.5194/egusphere-2023-201
Preprint. Discussion started: 16 February 2023

are associated with space weather events including radio blackout or polar cap absorption event that are resulting from solar proton enhancement and solar energetic particle events. The results from current study also indicate that analyzed SRBs were associate by ionospheric disturbances as demonstrated by TEC enhancement. The findings of this study demonstrate that it is possible to track well the progress of solar cycle 25 and forecast the intensity of associated space weather phenomena by analyzing and characterizing the physical features accompanying Type II SRBs observed from the ground (Ndacyayisenga et al., 2021a).

Author contributions. T. Ndacyayisenga, Jean Uwamahoro and D. Okoh conceived the presented idea and the design of the study. T. Ndacyayisenga manually gathered the data used. C. Monstein and D. Okoh, helped in programming for data analysis. Analysis and intrepretation of the results are done by T Ndacyayisenga who later drafted the manuscript. This manuscript is reviewed by Jean Uwamahoro, J. C Uwamahoro, Rabiu Babatunde, D. Okoh, K. Sasikumar Raja and C. Kwisanga.

Competing interests. The authors declare that the research was conducted in the absence of any commercial or financial relationships that could be created as a potential conflict of interest.

Acknowledgements. This work was supported by International Science Programme (ISP) through Rwanda Astrophysics, Space and Climate Science Research Group (RASCSRG) and Centre for atmospheric Research through National Space Research and Development Agency, Abuja, Nigeria. We thank FHNW, Institute for Data Science in Brugg/Windisch, Switzerland for hosting the e-Callisto network. The authors also thank the providers of all the data used from SOHO/LASCO; NOAA; GOES, SWPC, African Geodetic Reference Frame (http://afrefdata.org), WDC-SILSO and the UNAVCO Archive of GNSS Data (ftp://data-out.unavco.org). The author (C. Monstein) thanks the ISSI - Bern International Team of 'Why Ionospheric Dynamics and Structure Behave Differently in The African Sector' (the team leaders E. Yizengaw & K. Groves) for valuable discussions about part of the results that are included in this paper.

https://doi.org/10.5194/egusphere-2023-201
Preprint. Discussion started: 16 February 2023

References

Ahluwalia, H. S.: Forecast for sunspot cycle 25 activity, Advances in Space Research, 69, 794–797, https://doi.org/10.1016/j.asr.2021.09.035, 2022.

Amory-Mazaudier, C., Menvielle, M., Curto, J.-J., and Le Huy, M.: Recent Advances in Atmospheric, Solar-Terrestrial Physics and Space Weather From a North-South network of scientists [2006-2016] PART A: TUTORIAL, Sun and Geosphere, 12, 1–19, 2017.

Benz, A. O., Monstein, C., and Meyer, H.: Callisto A New Concept for Solar Radio Spectrometers, Sol. Phys., 226, 143–151, https://doi.org/10.1007/s11207-005-5688-9, 2005.

Benz, A. O., Monstein, C., Meyer, H., Manoharan, P. K., Ramesh, R., Altyntsev, A., Lara, A., Paez, J., and Cho, K. S.: A World-Wide Net of Solar Radio Spectrometers: e-CALLISTO, Earth Moon and Planets, 104, 277–285, https://doi.org/10.1007/s11038-008-9267-6, 2009.

Brajša, R., Verbanac, G., Bandić, M., Hanslmeier, A., Skokić, I., and Sudar, D.: A prediction for the 25th solar cycle maximum amplitude, Astronomische Nachrichten, 343, e13960, https://doi.org/10.1002/asna.202113960, 2022.

Brueckner, G. E., Howard, R. A., Koomen, M. J., Korendyke, C. M., Michels, D. J., Moses, J. D., Socker, D. G., Dere, K. P., Lamy, P. L., Llebaria, A., Bout, M. V., Schwenn, R., Simnett, G. M., Bedford, D. K., and Eyles, C. J.: The Large Angle Spectroscopic Coronagraph (LASCO), Sol. Phys., 162, 357–402, https://doi.org/10.1007/BF00733434, 1995.

Cairns, I. H., Knock, S. A., Robinson, P. A., and Kuncic, Z.: Type II Solar Radio Bursts: Theory and Space Weather Implications, Space Sci. Rev., 107, 27–34, https://doi.org/10.1023/A:1025503201687, 2003.

Cane, H. V. and Erickson, W. C.: Studies of Space Weather Using Solar Radio Bursts, in: From Clark Lake to the Long Wavelength Array: Bill Erickson's Radio Science, edited by Kassim, N., Perez, M., Junor, W., and Henning, P., vol. 345 of *Astronomical Society of the Pacific Conference Series*, p. 133, 2005.

Carley, E. P., Vilmer, N., Simões, P. J. A., and Ó Fearraigh, B.: Estimation of a coronal mass ejection magnetic field strength using radio observations of gyrosynchrotron radiation, A&A, 608, A137, https://doi.org/10.1051/0004-6361/201731368, 2017.

Chernov, G. and Fomichev, V.: On the Issue of the Origin of Type II Solar Radio Bursts, ApJ, 922, 82, https://doi.org/10.3847/1538-4357/ac1f32, 2021.

Cho, K. S., Lee, J., Gary, D. E., Moon, Y. J., and Park, Y. D.: Magnetic Field Strength in the Solar Corona from Type II Band Splitting, ApJ, 665, 799–804, https://doi.org/10.1086/519160, 2007.

Cho, K.-S., Gopalswamy, N., Kwon, R.-Y., Kim, R.-S., and Yashiro, S.: A HIGH-FREQUENCY TYPE II SOLAR RADIO BURST ASSOCIATED WITH THE 2011 FEBRUARY 13 CORONAL MASS EJECTION, The Astrophysical Journal, 765, 148, https://doi.org/10.1088/0004-637X/765/2/148, 2013.

Cunha-Silva, R. D., Fernandes, F. C. R., and Selhorst, C. L.: Solar type II radio bursts associated with CME expansions as shown by EUV waves, A& A, 578, A38, https://doi.org/10.1051/0004-6361/201425388, 2015.

Du, Z. L.: The solar cycle: predicting the peak of solar cycle 25, Astrophysics and Space Science, 365, 104, https://doi.org/10.1007/s10509-020-03818-1, 2020.

Dulk, G. A. and McLean, D. J.: Coronal magnetic fields., Sol. Phys., 57, 279–295, https://doi.org/10.1007/BF00160102, 1978.

Fleishman, G. D., Gary, D. E., Chen, B., Kuroda, N., Yu, S., and Nita, G. M.: Decay of the coronal magnetic field can release sufficient energy to power a solar flare, Science, 367, 278–280, https://doi.org/10.1126/science.aax6874, 2020.

Gopalswamy, N.: Coronal Mass Ejections and Solar Radio Emissions, in: Planetary, Solar and Heliospheric Radio Emissions (PRE VII), edited by Rucker, H. O., Kurth, W. S., Louarn, P., and Fischer, G., pp. 325–342, 2011.

https://doi.org/10.5194/egusphere-2023-201
Preprint. Discussion started: 16 February 2023

Gopalswamy, N. and Yashiro, S.: THE STRENGTH AND RADIAL PROFILE OF THE CORONAL MAGNETIC FIELD FROM THE STANDOFF DISTANCE OF A CORONAL MASS EJECTION-DRIVEN SHOCK, The Astrophysical Journal Letters, 736, L17, https://doi.org/10.1088/2041-8205/736/1/L17, 2011.

Gopalswamy, N., Nitta, N., Akiyama, S., Mäkelä, P., and Yashiro, S.: CORONAL MAGNETIC FIELD MEASUREMENT FROM EUV IMAGES MADE BY THE SOLAR DYNAMICS OBSERVATORY, The Astrophysical Journal, 744, 72, https://doi.org/10.1088/0004-637x/744/1/72, 2011.

Gopalswamy, N., Xie, H., Mäkelä, P., Yashiro, S., Akiyama, S., Uddin, W., Srivastava, A., Joshi, N., Chandra, R., Manoharan, P., Mahalakshmi, K., Dwivedi, V., Jain, R., Awasthi, A., Nitta, N., Aschwanden, M., and Choudhary, D.: Height of shock formation in the solar corona inferred from observations of type II radio bursts and coronal mass ejections, Advances in Space Research, 51, 1981–1989, https://doi.org/https://doi.org/10.1016/j.asr.2013.01.006, 2013.

Gopalswamy, N., Yashiro, S., Mäkelä, P., Xie, H., Akiyama, S., and Monstein, C.: Extreme Kinematics of the 2017 September 10 Solar Eruption and the Spectral Characteristics of the Associated Energetic Particles, The Astrophysical Journal, 863, L39, https://doi.org/10.3847/2041-8213/aad86c, 2018.

Grechnev, V. V., Afanasyev, A. N., Uralov, A. M., Chertok, I. M., Eselevich, M. V., Eselevich, V. G., Rudenko, G. V., and Kubo, Y.: Coronal Shock Waves, EUV Waves, and Their Relation to CMEs. III. Shock-Associated CME/EUV Wave in an Event with a Two-Component EUV Transient, Sol. Phys., 273, 461–477, https://doi.org/10.1007/s11207-011-9781-y, 2011.

Kallunki, J., McKay, D., and Tornikoski, M.: First Type III Solar Radio Bursts of Solar Cycle 25, Sol. Phys., 296, 57, https://doi.org/10.1007/s11207-021-01790-9, 2021.

Kavanagh, A., Marple, S., Honary, F., McCrea, I., and Senior, A.: On solar protons and polar cap absorption: constraints on an empirical relationship, Annales Geophysicae, 22, 1133–1147, https://doi.org/10.5194/angeo-22-1133-2004, 2004.

Kim, R.-S., Gopalswamy, N., Moon, Y.-J., Cho, K.-S., and Yashiro, S.: MAGNETIC FIELD STRENGTH IN THE UPPER SOLAR CORONA USING WHITE-LIGHT SHOCK STRUCTURES SURROUNDING CORONAL MASS EJECTIONS, The Astrophysical Journal, 746, 118, https://doi.org/10.1088/0004-637x/746/2/118, 2012.

Kouloumvakos, A., Rouillard, A., Warmuth, A., Magdalenic, J., Jebaraj, I. C., Mann, G., Vainio, R., and Monstein, C.: Coronal Conditions for the Occurrence of Type II Radio Bursts, ApJ, 913, 99, https://doi.org/10.3847/1538-4357/abf435, 2021.

Kumari, A., Ramesh, R., Kathiravan, C., and Wang, T. J.: Addendum to: Strength of the Solar Coronal Magnetic Field - A Comparison of Independent Estimates Using Contemporaneous Radio and White-Light Observations, Sol. Phys., 292, 177, https://doi.org/10.1007/s11207-017-1203-3, 2017.

Kumari, A., Ramesh, R., Kathiravan, C., Wang, T. J., and Gopalswamy, N.: Direct Estimates of the Solar Coronal Magnetic Field Using Contemporaneous Extreme-ultraviolet, Radio, and White-light Observations, The Astrophysical Journal, 881, 24, https://doi.org/10.3847/1538-4357/ab2adf, 2019.

Kumari, A., Morosan, D. E., and Kilpua, E. K. J.: On the Occurrence of Type IV Solar Radio Bursts in Solar Cycle 24 and Their Association with Coronal Mass Ejections, ApJ, 906, 79, https://doi.org/10.3847/1538-4357/abc878, 2021.

Lata Soni, S., Ebenezer, E., and lal Yadav, M.: Multi-wavelength analysis of CME-driven shock and Type II solar radio burst band-splitting, Astrophys Space Sci, 366, 31, https://doi.org/10.1007/s10509-021-03933-7, 2021.

Leblanc, Y., Dulk, G. A., and Bougeret, J.-L.: Tracing the Electron Density from the Corona to 1au, Sol. Phys., 183, 165–180, https://doi.org/10.1023/A:1005049730506, 1998.

https://doi.org/10.5194/egusphere-2023-201
Preprint. Discussion started: 16 February 2023

Maguire, C. A., Carley, E. P., McCauley, J., and Gallagher, P. T.: Evolution of the Alfvén Mach number associated with a coronal mass ejection shock, A & A, 633, A56, https://doi.org/10.1051/0004-6361/201936449, 2020.

Maia, D., Pick, M., Vourlidas, A., and Howard, R.: Development of Coronal Mass Ejections: Radio Shock Signatures, The Astrophysical Journal, 528, L49–L51, https://doi.org/10.1086/312421, 2000.

Mann, G., Vocks, C., Warmuth, A., Magdalenic, J., Bisi, M., Carley, E., Dabrowski, B., Gallagher, P., Krankowski, A., Maty-jasiak, B., Rotkaehl, H., and Zucca, P.: Excitation of Langmuir waves at shocks and solar type II radio bursts, A&A, 660, A71, https://doi.org/10.1051/0004-6361/202142201, 2022.

Minta, F. N., Nozawa, S., Kamen, K., Elsaid, A., and Ayman, A.: Assessing the spectral characteristics of band splitting type II radio bursts observed by CALLISTO spectrometers, arXiv e-prints, arXiv:2301.13839, https://doi.org/10.48550/arXiv.2301.13839, 2023.

Mitra, A. P.: Polar Cap Absorption Events, pp. 252–278, Springer Netherlands, Dordrecht, https://doi.org/10.1007/978-94-010-2231-6_11, 1974.

Ndacyayisenga, T., Umuhire, A. C., Uwamahoro, J., and Monstein, C.: Space weather study through analysis of solar radio bursts detected by a single-station CALLISTO spectrometer, Annales Geophysicae, 39, 945–959, https://doi.org/10.5194/angeo-39-945-2021, 2021a.

Ndacyayisenga, T., Uwamahoro, J., Sasikumar Raja, K., and Monstein, C.: A statistical study of solar radio Type III bursts and space weather implication, Advances in Space Research, 67, 1425–1435, https://doi.org/https://doi.org/10.1016/j.asr.2020.11.022, 2021b.

Nedal, M., Mahrous, A., and Youssef, M.: Predicting the arrival time of CME associated with type-II radio burst using neural networks technique, Ap & Space Sci., 364, 161, https://doi.org/10.1007/s10509-019-3651-8, 2019.

Newkirk, Gordon, J.: Structure of the Solar Corona, Annu. Rev. Astron. Astrophys., 5, 213, https://doi.org/10.1146/annurev.aa.05.090167.001241, 1967.

Nindos, A.: Incoherent Solar Radio Emission, Frontiers in Astronomy and Space Sciences, 7, 57, https://doi.org/10.3389/fspas.2020.00057, 2020.

Nindos, A., Aurass, H., Klein, K. L., and Trottet, G.: Radio Emission of Flares and Coronal Mass Ejections. Invited Review, Sol. Phys., 253, 3–41, https://doi.org/10.1007/s11207-008-9258-9, 2008.

Payne-Scott, R., Yabsley, D. E., and Bolton, J. G.: Relative Times of Arrival of Bursts of Solar Noise on Different Radio Frequencies, Nature, 160, 256–257, https://doi.org/10.1038/160256b0, 1947.

Perrone, L., Alfonsi, L., Romano, V., and Franceschi, G.: Polar cap absorption events of November 2001 at Terra Nova Bay, Antarctica, Annales Geophysicae, 22, 1633–1648, https://doi.org/10.5194/angeo-22-1633-2004, 2004.

Pick, M., Forbes, T. G., Mann, G., Cane, H. V., Chen, J., Ciaravella, A., Cremades, H., Howard, R. A., Hudson, H. S., Klassen, A., Klein, K. L., Lee, M. A., Linker, J. A., Maia, D., Mikic, Z., Raymond, J. C., Reiner, M. J., Simnett, G. M., Srivastava, N., Tripathi, D., Vainio, R., Vourlidas, A., Zhang, J., Zurbuchen, T. H., Sheeley, N. R., and Marqué, C.: Multi-Wavelength Observations of CMEs and Associated Phenomena. Report of Working Group F, Space Sci. Rev., 123, 341–382, https://doi.org/10.1007/s11214-006-9021-1, 2006.

Ramesh, R., Kathiravan, C., and Sastry, C. V.: ESTIMATION OF MAGNETIC FIELD IN THE SOLAR CORONAL STREAMERS THROUGH LOW FREQUENCY RADIO OBSERVATIONS, The Astrophysical Journal, 711, 1029–1032, https://doi.org/10.1088/0004-637x/711/2/1029, 2010.

Ranta, H., Ranta, A., Yousef, S. M., Burns, J., and Stauning, P.: D-region observations of polar cap absorption events during the EISCAT operation in 1981-1989., Journal of Atmospheric and Terrestrial Physics, 55, 751–766, https://doi.org/10.1016/0021-9169(93)90018-T, 1993.

https://doi.org/10.5194/egusphere-2023-201
Preprint. Discussion started: 16 February 2023

Reid, H. A. S. and Ratcliffe, H.: A review of solar type III radio bursts, Research in Astronomy and Astrophysics, 14, 773–804, https://doi.org/10.1088/1674-4527/14/7/003, 2014.

Saito, K., Poland, A. I., and Munro, R. H.: A study of the background corona near solar minimum., Sol. Phys., 55, 121–134, https://doi.org/10.1007/BF00150879, 1977.

Salmane, H., Weber, R., Abed-Meraim, K., Klein, K.-L., and Bonnin, X.: A method for the automated detection of solar radio bursts in dynamic spectra, Journal of Space Weather and Space Climate, 8, A43, https://doi.org/10.1051/swsc/2018028, 2018.

Sarp, V., Kilcik, A., Yurchyshyn, V., Rozelot, J. P., and Ozguc, A.: Prediction of solar cycle 25: a non-linear approach, MNRAS, 481, 2981–2985, https://doi.org/10.1093/mnras/sty2470, 2018.

Sasikumar Raja, K., Ramesh, R., Hariharan, K., Kathiravan, C., and Wang, T. J.: An Estimate of the Magnetic Field Strength Associated with a Solar Coronal Mass Ejection from Low Frequency Radio Observations, ApJ, 796, 56, https://doi.org/10.1088/0004-637X/796/1/56, 2014.

Sasikumar Raja, K., Venkata, S., Singh, J., and Raghavendra Prasad, B.: Solar coronal magnetic fields and sensitivity requirements for spectropolarimetry channel of VELC onboard Aditya-L1, Advances in Space Research, 69, 814–822, https://doi.org/10.1016/j.asr.2021.10.053, 2022.

Seemala, G. K. and Valladares, C. E.: Statistics of total electron content depletions observed over the South American continent for the year 2008, Radio Science, 46, https://doi.org/https://doi.org/10.1029/2011RS004722, 2011.

Shea, M. A. and Smart, D. F.: Solar proton event patterns: the rising portion of five solar cycles, Advances in Space Research, 29, 325–330, https://doi.org/10.1016/S0273-1177(01)00592-0, 2002.

Smerd, S. F., Sheridan, K. V., and Stewart, R. T.: On Split-Band Structure in Type II Radio Bursts from the Sun (presented by S.F. Smerd), in: Coronal Disturbances, edited by Newkirk, G. A., vol. 57, p. 389, 1974.

Smerd, S. F., Sheridan, K. V., and Stewart, R. T.: Split-Band Structure in Type II Radio Bursts from the Sun, Astrophys. Lett., 16, 23, 1975.

Smith, A. R. A., Beggan, C. D., Macmillan, S., and Whaler, K. A.: Climatology of the Auroral Electrojets Derived From the Along-Track Gradient of Magnetic Field Intensity Measured by POGO, Magsat, CHAMP, and Swarm, Space Weather, 15, 1257–1269, https://doi.org/10.1002/2017SW001675, 2017.

Su, W., Li, T. M., Cheng, X., Feng, L., Zhang, P. J., Chen, P. F., Ding, M. D., Chen, L. J., Guo, Y., Wang, Y., Li, D., and Zhang, L. Y.: Quantifying the Magnetic Structure of a Coronal Shock Producing a Type II Radio Burst, The Astrophysical Journal, 929, 175, https://doi.org/10.3847/1538-4357/ac5fac, 2022.

SW: SOLAR CYCLE UPDATE. Retrieved from https://spaceweather.com/archive.php?view=1&day=12&month=01&year=2022, Accessed on 18 July 2022, p. 1, 2022.

Tan, B.: Multi-timescale solar cycles and the possible implications, Astrophysics and Space Science, 332, 65–72, https://doi.org/10.1007/s10509-010-0496-6, 2011.

Tan, B., Chen, N., Yang, Y.-H., Tan, C., Masuda, S., Chen, X., and Misawa, H.: Solar Fast-drifting Radio Bursts in an X1.3 Flare on 2014 April 25, The Astrophysical Journal, 885, 90, https://doi.org/10.3847/1538-4357/ab4718, 2019.

Temmer, M., Veronig, A. M., Kontar, E. P., Krucker, S., and Vršnak, B.: Combined STEREO/RHESSI Study of Coronal Mass Ejections Acceleration and Particle Acceleration in Solar Flares, The Astrophysical Journal, 712, 1410–1420, https://doi.org/10.1088/0004-637x/712/2/1410, 2010.

https://doi.org/10.5194/egusphere-2023-201
Preprint. Discussion started: 16 February 2023

Umuhire, A. C., Gopalswamy, N., Uwamahoro, J., Akiyama, S., Yashiro, S., and Mäkelä, P.: Properties of High-Frequency Type II Radio Bursts and Their Relation to the Associated Coronal Mass Ejections, Sol. Phys., 296, 27, https://doi.org/10.1007/s11207-020-01743-8, 2021.

Vasanth, V., Umapathy, S., Vršnak, B., and Anna Lakshmi, M.: Characteristics of Type-II Radio Bursts Associated with Flares and CMEs, Sol. Phys., 273, 143–162, https://doi.org/10.1007/s11207-011-9854-y, 2011.

Vasanth, V., Umapathy, S., Vršnak, B., Žic, T., and Prakash, O.: Investigation of the Coronal Magnetic Field Using a Type II Solar Radio Burst, Sol. Phys., 289, 251–261, https://doi.org/10.1007/s11207-013-0318-4, 2014.

Vemareddy, P., Démoulin, P., Sasikumar Raja, K., Zhang, J., Gopalswamy, N., and Vasantharaju, N.: Eruption of the EUV Hot Channel from the Solar Limb and Associated Moving Type IV Radio Burst, ApJ, 927, 108, https://doi.org/10.3847/1538-4357/ac4dfe, 2022.

Vourlidas, A., Carley, E. P., and Vilmer, N.: Radio Observations of Coronal Mass Ejections: Space Weather Aspects, Frontiers in Astronomy and Space Sciences, 7, 43, https://doi.org/10.3389/fspas.2020.00043, 2020.

Vršnak, B., Aurass, H., Magdalenić, J., and Gopalswamy, N.: Band-splitting of coronal and interplanetary type II bursts. I. Basic properties, A & A, 377, 321–329, https://doi.org/10.1051/0004-6361:20011067, 2001.

Vršnak, B., Magdalenić, J., Aurass, H., and Mann, G.: Band-splitting of coronal and interplanetary type II bursts. II. Coronal magnetic field and Alfvén velocity, A & A, 396, 673–682, https://doi.org/10.1051/0004-6361:20021413, 2002.

Wild, J. P. and McCready, L. L.: Observations of the Spectrum of High-Intensity Solar Radiation at Metre Wavelengths. I. The Apparatus and Spectral Types of Solar Burst Observed, Australian Journal of Scientific Research A Physical Sciences, 3, 387, https://doi.org/10.1071/CH9500387, 1950.

Wild, J. P., Smerd, S. F., and Weiss, A. A.: Solar Bursts, Ann. Rev. Astron and Astrophys., 1, 291, https://doi.org/10.1146/annurev.aa.01.090163.001451, 1963.

Zucca, P., Morosan, D. E., Rouillard, A. P., Fallows, R., Gallagher, P. T., Magdalenic, J., Klein, K. L., Mann, G., Vocks, C., Carley, E. P., Bisi, M. M., Kontar, E. P., Rothkaehl, H., Dabrowski, B., Krankowski, A., Anderson, J., Asgekar, A., Bell, M. E., Bentum, M. J., Best, P., Blaauw, R., Breitling, F., Broderick, J. W., Brouw, W. N., Brüggen, M., Butcher, H. R., Ciardi, B., de Geus, E., Deller, A., Duscha, S., Eislöffel, J., Garrett, M. A., Grießmeier, J. M., Gunst, A. W., Heald, G., Hoeft, M., Hörandel, J., Iacobelli, M., Juette, E., Karastergiou, A., van Leeuwen, J., McKay-Bukowski, D., Mulder, H., Munk, H., Nelles, A., Orru, E., Paas, H., Pandey, V. N., Pekal, R., Pizzo, R., Polatidis, A. G., Reich, W., Rowlinson, A., Schwarz, D. J., Shulevski, A., Sluman, J., Smirnov, O., Sobey, C., Soida, M., Thoudam, S., Toribio, M. C., Vermeulen, R., van Weeren, R. J., Wucknitz, O., and Zarka, P.: Shock location and CME 3D reconstruction of a solar type II radio burst with LOFAR, A & A, 615, A89, https://doi.org/10.1051/0004-6361/201732308, 2018.